TITLE

Visualizing subcellular structures in neuronal tissue with expansion microscopy

AUTHORS

Logan A. Campbell[1*], Katy E. Pannoni[1*], Niesha A. Savory[2], Dinesh Lal[3], Shannon Farris[1-4#]

AFFILIATIONS

[1]Center for Neurobiology Research, Fralin Biomedical Research Institute, Virginia Tech Carilion, Roanoke, VA, 24016, USA.
[2]School of Neuroscience, Virginia Tech, Blacksburg, VA, 24016, USA.
[3]Virginia Tech Carilion School of Medicine, Roanoke, VA, 24016, USA.
[4]Department of Biomedical Sciences & Pathobiology, Virginia-Maryland College of Veterinary Medicine, Virginia Tech, Blacksburg, VA, 24061, USA.

[*]Authors contributed equally
[#]Lead Contact Farrissl@vtc.vt.edu

Word Count: Abstract 174; Introduction, Results, Discussion 4,029
Figures: 7; Tables: 3

KEYWORDS Expansion microscopy, hippocampus, subcellular localization, dendrites, spines, mitochondria, Golgi apparatus,

ABSTRACT

Protein expansion microscopy (proExM) is a powerful technique that crosslinks proteins to a swellable hydrogel to physically expand and optically clear biological samples. The resulting increased resolution (~70 nm) and physical separation of labeled proteins make it an attractive tool for studying the localization of subcellular organelles in densely packed tissues, such as the brain. However, the digestion and expansion process greatly reduces fluorescence signals making it necessary to optimize ExM conditions per sample for specific end goals. Here we describe a proExM workflow optimized for resolving subcellular organelles (mitochondria and the Golgi apparatus) and reporter-labeled spines in fixed mouse brain tissue. By directly comparing proExM staining and digestion protocols, we found that immunostaining before proExM and using a proteinase K based digestion for 8 hours consistently resulted in the best fluorescence signal to resolve subcellular organelles while maintaining sufficient reporter labeling to visualize spines and trace individual neurons. With these methods, we more accurately quantified mitochondria size and number and better visualized Golgi ultrastructure in reconstructed CA2 neurons of the hippocampus.

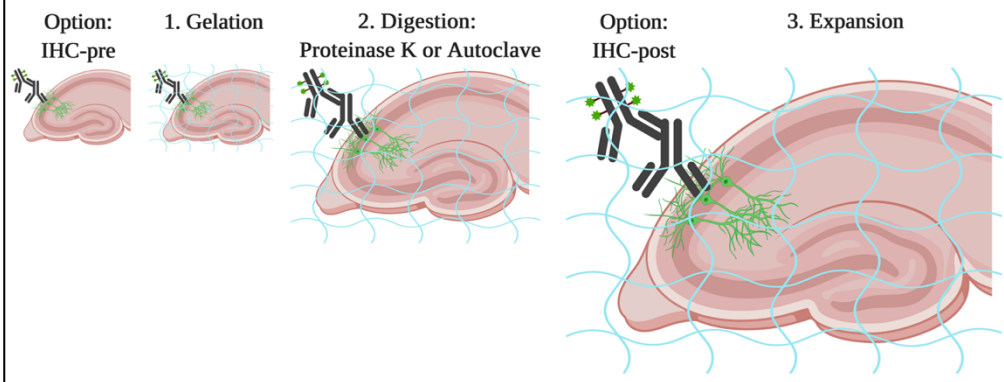

Figure 1: ExM workflow for visualizing subcellular organelles in fixed brain tissue. Schematic of immunostaining and proExM workflows tested to optimize visualization of organelles in genetically-labeled neurons.

INTRODUCTION

Protein retention expansion microscopy (proExM) is a powerful tool that crosslinks proteins to a swellable hydrogel to optically clear and physically expand tissues up to ~4-fold in volume[1,2]. Because expansion physically separates crosslinked moieties, this technology is particularly useful for visualizing subcellular structures in densely packed tissues, such as the brain. However, one consequence of tissue expansion is a decrease in the fluorescence intensity of labeled proteins primarily due to the digestion process and the dilution of fluorescence signal per unit volume. Various ExM protocols have described different methods for improving fluorescence retention, primarily by modifying fixation, crosslinking, and/or digestion conditions to preserve protein epitopes[2–8]. One common ExM protocol uses a strong protease-based digestion (proteinase K[2]), but other gentler proteases have also been used (LysC[2,3]), as well as a combination of heat and detergents in place of proteases (e.g. autoclave in an alkaline buffer[2–5]).

Immunostaining can also be done before or after ExM to boost fluorescence[2,3] (Fig. 1), although results are often dependent on the protein epitope and the quality of antibody staining. To improve antibody staining in brain tissue, antigen retrieval is often performed prior to immunostaining via boiling tissue in water or heating tissue in a citrate buffer (pH 6) to expose protein epitopes and reduce nonspecific staining. Here we set out to compare ExM immunostaining and digestion conditions for fluorescently labeled subcellular organelles in perfused brain sections using antibodies that either require or do not require antigen retrieval (COX4-labeling of mitochondria and GOLGA5-labeling of Golgi, respectively). Visualizing the spatial organization of organelles within compartmentalized cells, such as neurons, is important for understanding their function, thus we paid particular attention to conditions that maintained fluorescence signal from genetically-encoded reporters (i.e. enhanced green fluorescent protein, EGFP, and tdTomato). We found that performing IHC, with or without antigen retrieval, prior to ExM with proteinase K digestion for 8 hours best preserves fluorescence signal for co-visualizing subcellular organelles and neuronal morphology, including spines. Further, we report

our optimized conditions for antibodies against widely used reporters and conclude with protocol considerations for achieving specific end goals.

RESULTS

Proteinase K digestion time impacts fluorescence intensity and expansion factor

Sufficient digestion or homogenization (also referred to as hydrolysis in some protocols) is required to prevent sample distortion during expansion and is highly dependent on digestion conditions, including time, temperature, pH, buffer composition and enzyme quality[1,3,9]. Varying digestion time impacts fluorescence intensity[1] and how much the tissue expands in water, or the expansion factor[5]. To determine the effect of digestion time on the fluorescence intensity of the Amigo2-EGFP reporter line, which predominantly labels hippocampal area CA2 neurons, we performed a time course of enzymatic digestion with proteinase K as described in the proExM protocol[3]. Initially, we performed the time course on 40-micron vibratome cut sections from perfused adult Amigo2-EGFP mouse brains. Hydrogels were digested for 2, 4, 8 or 16 hours at room temperature. Unfortunately, there was insufficient EGFP signal remaining at the 8 and 16 hour timepoints to directly compare hydrogels across conditions (data not shown). We then repeated the experiment on sections immunostained for GFP prior to ExM and imaged the resulting gels with identical acquisition parameters to directly compare fluorescence intensities and expansion factors (Fig. 2). Importantly, we measured micro expansion factors, or the degree to which cell soma areas expanded versus the commonly reported macro expansion factors calculated by measuring how much the hydrogel expands. We found that average fluorescence intensities diminished as the length of digestion time increased (one-way ANOVA; F-stat: 20.96, p-value: 8.17E-14. N = two animals, 1-2 sections per animal per time point; 159 total cells, 32 ± 4 cells per time point, Fig. 2AB). Further, we found that average expansion factors increased as length of digestion time increased (one-way ANOVA; F-stat: 21.07, p-value: 4.26E-11, Fig. 2CD), resulting in an inverse relationship between fluorescence intensity and expansion factor (Fig. 2E). Interestingly, we did not detect significant decreases in fluorescence intensities from pairwise comparisons between the 8-hr digestion and the 2- or 4-hr digestions (p=0.90 and 0.55, respectively, Tukey's post hoc test, Fig. 2D), despite significant increases in expansion factors between the same comparisons (p=0.001 for each). These data indicate that 8-hr digestion retains the most fluorescence for a sizable expansion factor (~3) that is not significantly different from the overnight expansion factor (p=0.18). However, we note that the fluorescence intensities reported here are corrected for background, and shorter digestion times have greater fluorescence background signal compared with longer digestion times (see Table 1). We also compared the cell area micro expansion factor to the extent that the tissue section expands (macro expansion factor) and found the macro expansion factor to be consistently greater than the micro expansion factor (Fig. 2F). Regardless of digestion time, we were able to successfully acquire robust fluorescent images at each time point, including overnight (Fig. 2G), as long as immunostaining was performed prior to ExM.

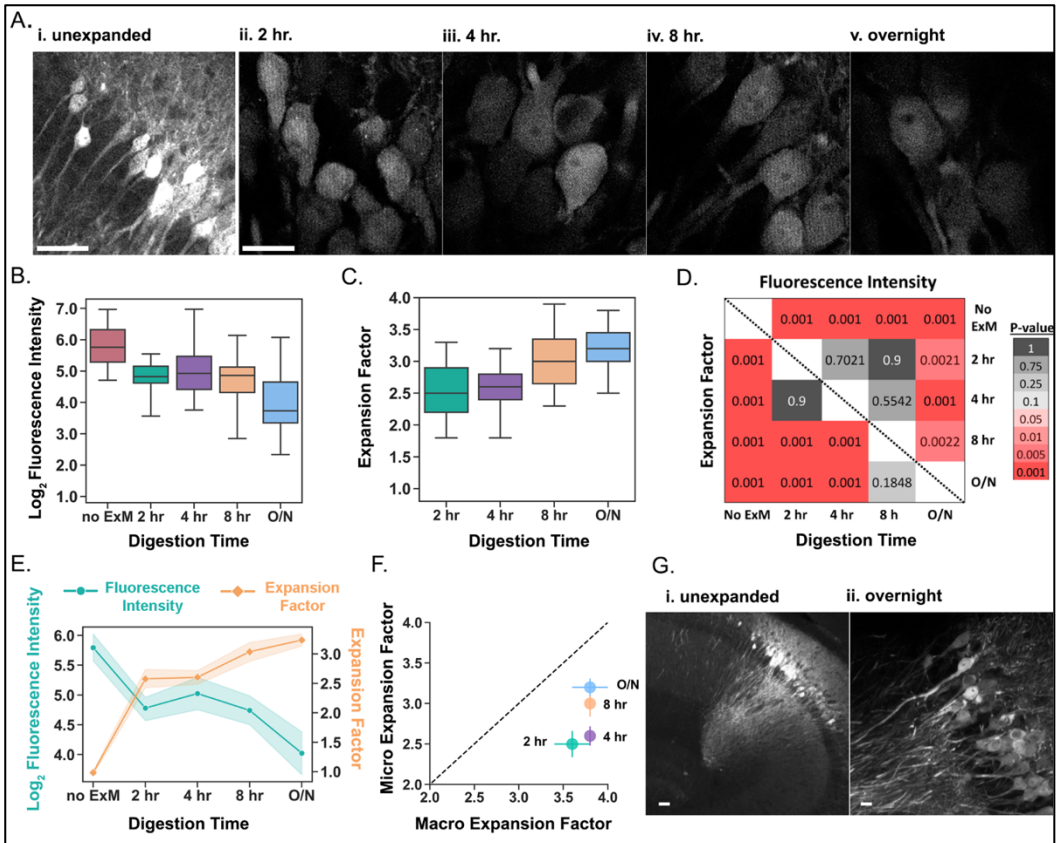

Figure 2: The effect of Proteinase K digestion time on fluorescence intensity and expansion factor.
A) Representative single z-section images of unexpanded (i) and expanded GFP+ CA2 neurons after 2-hour (ii), 4-hour (iii), 8-hour (iv), or overnight (v) digestion with Proteinase K. Image acquisition parameters were identical for each condition, except for the unexpanded condition.
B) GFP fluorescence intensity measured in the cell soma after the different digestion times. Fluorescence was corrected for background and $\log_2$ transformed. Line represents the median. Digestion time had a significant effect on GFP fluorescence (one-way ANOVA; F-stat: 20.96, p-value: 8.17E-14, 32 ± 4 cells per time point from two animals, 159 total cells).
C) Expansion factor of the expanded cell somas in B. Expansion factors were calculated using cell soma areas relative to the average unexpanded cell soma area. Digestion time had a significant effect on expansion factor (one-way ANOVA; F-stat: 21.07, p-value: 4.26E-11).
D) Matrix of p-values visualizing the results of pairwise Tukey's post hoc tests comparing mean fluorescence (upper diagonal) or expansion factor (lower diagonal) at each digestion time point. Matrix is color coded by p-value (red = significant; grey = not significant; α=0.05).
E) Effect of digestion time on fluorescence intensity (cyan; left axis) and expansion factor (orange; right axis). Plot shows the mean and 95% confidence intervals from **B** and **C**.
F) Plot comparing cell area micro expansion factors versus tissue macro expansion factors. Error bars = 2*sem.
G) Unexpanded (i) and overnight expanded (ii) max-projection 10X confocal images of GFP+ CA2 cells. Images are the same as in **A**(i) and (v). Imaging parameters were optimized separately to obtain the best image of both. Scale bars = (**A**, **G**) 50 µm.

Cells expand equivalently, independent of section depth

Next we considered if the time-dependent effect of proteinase K on expansion factor and fluorescence intensity is impacted by tissue depth. We reasoned that cells near the surface may have greater access to proteinase K and/or fluorescently-labeled antibodies compared with cells deeper within tissue that may impact expansion factor and/or fluorescence intensity, respectively. To test this, we compared cell soma areas binned by Z-section depth (adjusted by hydrogel thickness) across digestion time points.

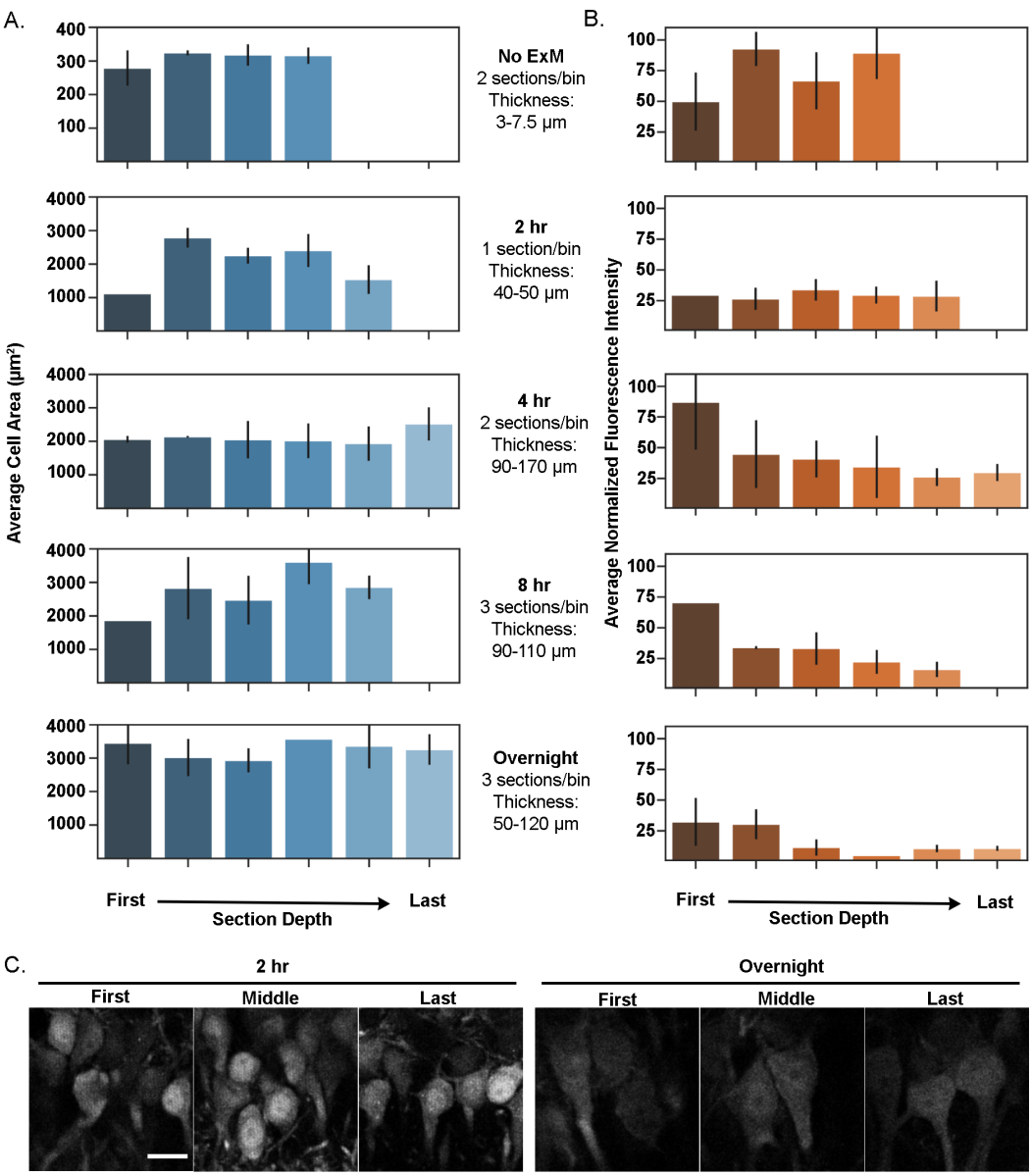

Figure 3: No appreciable effect of tissue depth on expansion factor.
A) Average cell soma area (in µm²) by Z section depth for unexpanded control and digestion conditions. Cell soma area was measured in the Z section with the widest soma diameter. Because of the overall increase in depth with expansion, cells were binned by Z section to achieve ~6 bins per time point. N = 32 ± 4 cells per time point.
B) Background subtracted average cell soma fluorescence by Z section depth. Binning of the data is the same as in A. The data are not $\log_2$ transformed as in Fig 2.
C) Representative confocal images of GFP+ CA2 cell somas after 2-hour (left panel) or overnight (right panel) digestion at three Z-section depths. Cell soma size and fluorescence is variable in the Z dimension in unexpanded conditions, which does not appreciably change under difference digestion conditions. Error bars show the standard deviation. Scale bar is 50µm.

We did not detect a systematic difference in cell soma area across z-section depth (Fig. 3), indicating that proteinase K equivalently digests 40-micron thick tissue, at least by the 2-hr time point. For some time points (e.g. 4- and 8-hrs) fluorescence intensity appeared brighter near the

121 surface compared with deeper sections (Fig. 3B). However, we note this is likely due to optical
122 limits, as fluorescence intensity was not brighter at the far-end surface that has equivalent access
123 to proteinase K and antibody solutions. We saw similar results with 100-micron thick tissue (data
124 not shown).
125
126 *Immunolabeled organelles are best resolved with IHC prior to ExM*
127 Protease digestion can decrease fluorescence intensity by impacting fluorescently-labeled
128 antibodies and/or target antigen availability. Thus, immunohistochemistry (IHC) labeling before
129 or after ExM (further referred to as IHC-pre and IHC-post, respectively) can be affected, but it is
130 unknown if they equally affect the fluorescence intensity of antibodies that require antigen
131 retrieval. Protease-free digestion protocols (e.g. detergent plus heat created in an autoclave liquid
132 cycle) have been shown to effectively digest hydrogels, and avoids protease-dependent depletion
133 of fluorescence intensity[3]. However, these protocols have not been tested with antibodies that
134 require antigen retrieval. In Figure 4, we directly compared COX4-mitochondria labeling after
135 protease (proteinase K) or autoclave (i.e. mild digestion) digestion ExM protocols[3]. We further
136 compared these digestion protocols with IHC performed pre (Fig. 4AB) or post ExM (Fig. 4CD).
137 Our optimized protocol for COX4 immunostaining on unexpanded sections (Fig. 4E) requires
138 antigen retrieval (boiling) prior to IHC, thus an antigen retrieval step was included for sections
139 bound for proteinase K digestion.
140
141 We detected COX4-labeled mitochondria using both proteinase K and autoclave digestion
142 ExM protocols (Fig. 4), however proteinase K digested gels performed better with IHC-pre, and
143 autoclave digested gels performed better with IHC-post. Compared with unexpanded COX4-
144 labeled mitochondria, expanded COX4-labeled mitochondria were on average slightly greater in
145 number per cell (ExM: 117.5 ± 5.6, No ExM: 95.8 ± 4.4) and smaller in size (mitochondria size:
146 ExM 0.001 ± 0.0, No ExM 0.003 ± 0.0) after normalizing to cell soma area (total mitochondria
147 area: ExM 422.5 ± 93.7, No ExM 123.8 ± 2.4) (Fig. 4G). To account for potential anisotropic
148 expansion of cell somas, we compared the ratio of nuclear area (measured via DAPI) to the cell
149 soma area (measured via reporter labeling) and found them to be similar on average with and
150 without ExM (ratio: ExM 0.357 ± 0.00, No ExM 0.347 ± 0.01; nuclear area: ExM 1,383.1 ±
151 93.5, No ExM 154.5 ± 7.8; soma area: ExM 3,869.5 ± 259.2, No ExM 443.3 ± 11.8), indicating
152 that the decrease in percent cytoplasmic area of mitochondria (Fig. 4I) is due to better
153 individually resolved expanded mitochondria.
154
155 In regards to reporter labeling, RFP fluorescence only fared well when IHC was done prior to
156 ExM, regardless of digestion method. Thus, for epitopes that require antigen retrieval and/or
157 reporter labeling, IHC-pre-ExM is the preferred method of choice. Note that antigen retrieval
158 diminishes reporter labeling (RFP and GFP) and explains the difference in RFP intensity
159 between autoclave (Fig. 4Aii) and proteinase K (Fig. 4Bii) digested gels. If only mitochondria
160 labeling is required, the autoclave digestion protocol performs well with IHC-post. The inferior

staining of COX4 with IHC-pre with autoclave digestion compared with IHC-pre with proteinase K digestion may be due to a lack of antigen retrieval in the former that is achieved by autoclave digestion. To provide a semi-quantitative measure for each method tested in Fig. 4A-D, we scored the COX4 and reporter images on a scale from 0-100 based equally on the brightness of the signal and the quality of the labeling, the latter of which took into account the amount of noise and how closely the labeling pattern matched the expected pattern from unexpanded samples. A higher score reflects greater fluorescence signal or better signal quality as illustrated in Fig. 4J. The ProK-pre condition best preserves both mitochondria and the reporter labels. This can be seen in the spinning disk confocal images in Fig. 4K-L. With this combination, we can observe individual mitochondria within reporter-labeled dendrites (Fig. 4L).

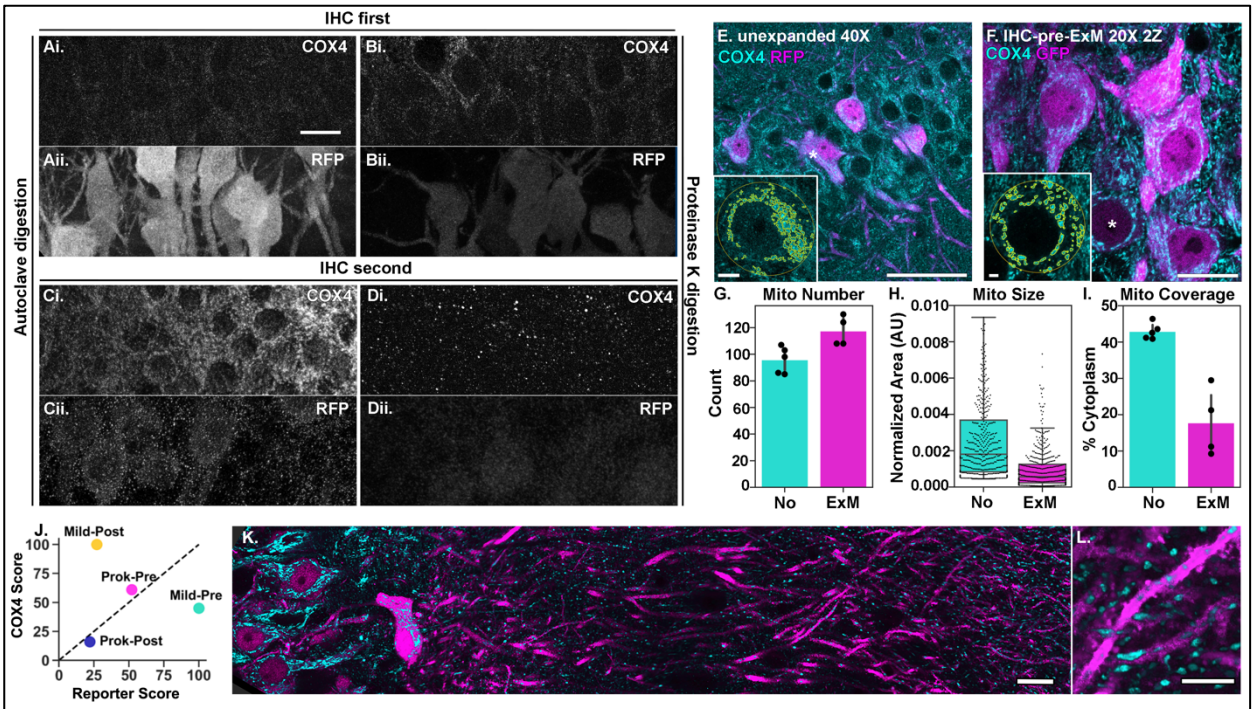

Figure 4: ProExM pipeline comparison for visualizing mitochondria.
A) 20X Max-projection image of a section immunostained for COX4 (i) and RFP (ii) pre-ExM with autoclave digestion. Images in panels A-D were acquired with identical imaging parameters to directly compare conditions. Brightness and contrast were adjusted to the same extent across the entire image.
B) 20X Max-projection image of a boiled section immunostained for COX4 (i) and RFP (ii) pre-ExM with overnight Proteinase K digestion.
C) 20X Max-projection image of a section immunostained for COX4 (i) and RFP (ii) post-ExM with autoclave digestion.
D) 20X Max-projection image of a boiled section immunostained for COX4 (i) and RFP (ii) post-ExM with overnight Proteinase K digestion
E) 40X Max-projection image from a subset of Z sections from a boiled, unexpanded section immunostained for COX4 and RFP. Inset is a single Z section from the indicated representative cell (white asterisk) with mitochondria outlined as quantified in **G-I**. Imaging parameters were optimized per condition in **E-F**.
F) 20X Max-projection image from a subset of Z sections from a boiled section immunostained for COX4 and GFP pre-ExM with overnight Proteinase K digestion as in **B**.
G) The average number of mitochondria per cell in unexpanded **(E)** and expanded **(F)** sections.
H) Mitochondria area per cell (normalized by soma area). Line reflects median and whiskers are twice the inner quartile range.
I) The average percent cytoplasm area (soma area - nuclear area) containing mitochondria. Note that ExM better resolves densely packed mitochondria, resulting in greater number, smaller sized, and fewer percent area per cell soma compared with non-ExM.
J) Semi quantitative histological scores comparing tested conditions in panels A-D.
K-L) Tile scan and high magnification image of mitochondria (cyan) in CA2 neurons and distal dendrites (magenta) with the conditions in **F**. Scale bars: 50 µm (**A**,**E**,**F**,**K**), 20 µm (**L**) and 5 µm (insets).

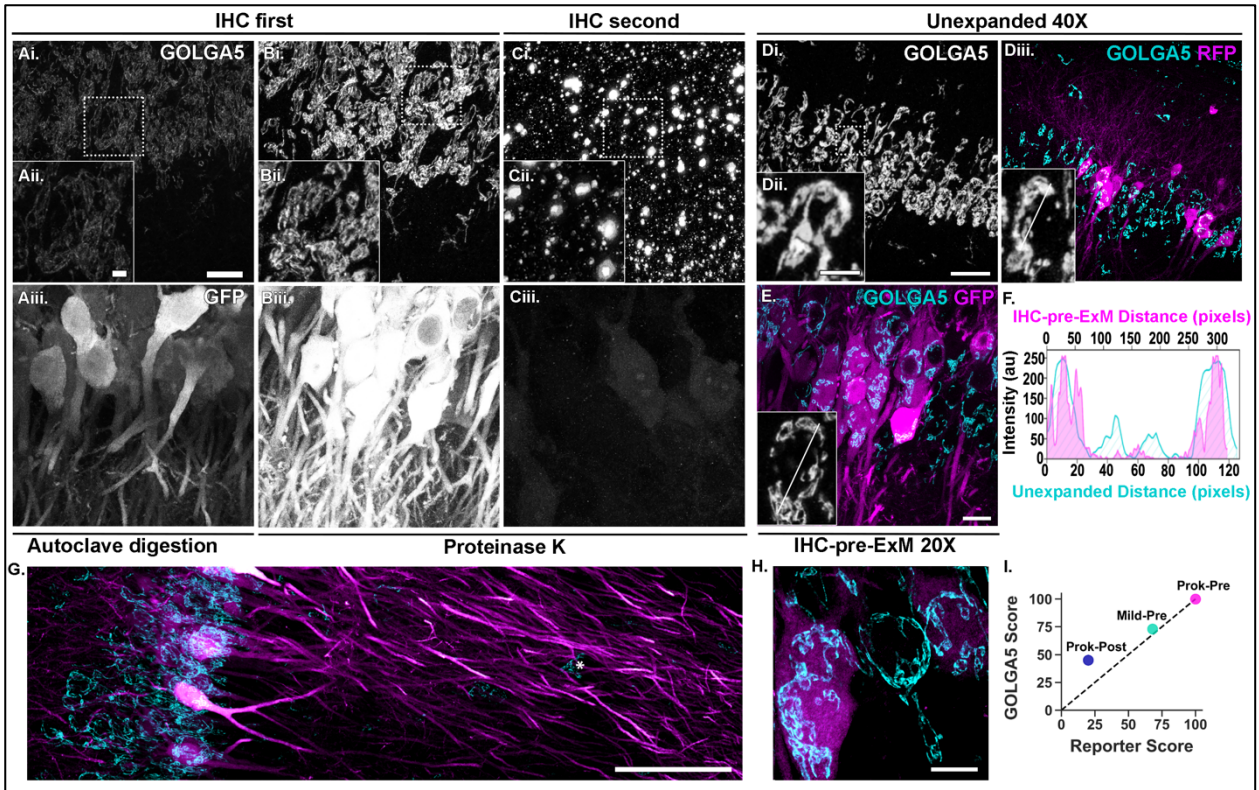

Figure 5: ProExM pipeline comparison for visualizing Golgi.
A) 20X Max-projection image of a section immunostained for GOLGA5 (i) and GFP (iii) pre-ExM with autoclave digestion. (ii) Insets are zoomed images of the dotted box in (i). Images in panels **A**-**C** were acquired with identical imaging parameters to directly compare conditions. Brightness and contrast were adjusted to the same extent across the entire image.
B) 20X Max-projection image of a section immunostained for GOLGA5 (i) and GFP (iii) pre-ExM with overnight Proteinase K digestion.
C) 20X Max-projection image of a section immunostained for GOLGA5 (i) and GFP (iii) post-ExM with overnight Proteinase K digestion.
D) 40X Max-projection of a subset of Z sections from an unexpanded section immunostained for GOLGA5 (i) and RFP (iii). Imaging parameters were optimized per condition in **D**-**E**.
E) 20X Max-projection of a subset of Z sections from image in (**B**) immunostained pre-ExM with overnight Proteinase K digestion. Note the increase in Golgi complexity that is resolved with autoclave or Proteinase K digested gels compared with unexpanded sections, although fluorescence intensity was better retained with Proteinase K digestion.
F) Line plot profile showing the fluorescence intensity of unexpanded Golgi (cyan) and Golgi after IHC-pre-ExM with Proteinase K digestion (magenta). Measured Golgi are insets in **D**iii and **E**.
G-H) Tile scan and high magnification image of GOLGA5 staining in CA2 neurons with the conditions in **E**. Note the lack of GOLGA5 signal in CA2 dendrites except that from glial cells (asterisk).
I) Semi quantitative histological scores comparing tested conditions in panels A-C.
Scale bars: 50 µm (**A**i, **D**i, **E**),10 µm (**A**ii, **D**ii), 200 µm (**G**) and 25 µm (**H**).

We next compared the proteinase K and autoclave ExM protocols with GOLGA5-immunolabeling of Golgi apparatus (Fig. 5), which does not require antigen retrieval. Consistent with our COX4 results, GOLGA5-labeled Golgi were detected with either proteinase K or autoclave digested protocols. Golgi in expanded sections were well resolved and revealed complex Golgi structure compared with Golgi in unexpanded sections (Fig. 5F). In contrast to our COX4 results, GOLGA5-labeling fared well in both IHC-pre-ExM digestion conditions, likely due to robust GOLGA5-labeling in unboiled sections. Similar to COX4, GOLGA5-labeling post-ExM with proteinase K digestion was unsuccessful. IHC-pre with autoclave digestion was not tested. As with RFP reporter labeling, GFP reporter labeling also fared well with IHC-pre and autoclave digestion, albeit at lower intensities than proteinase K digestion. Thus, GFP and RFP fluorescence retention are comparable when antibody-labeled prior to ExM

and they retain more fluorescence with proteinase K digestion compared with autoclave digestion. It is important to note that we detect qualitative differences in the ability of different reporter antibodies to detect spines, with and without ExM (see Table 3). Using the Prok-pre conditions, we were able to determine that there is no GOLGA5 labeled Golgi localized CA2 dendrites (Fig. 5G), despite clear GOLGA5 labeled Golgi in CA2 cell bodies (Fig. 5G-H). The GOLGA5 signal and reporter signal were semi-quantitatively scored as described above for mitochondria (Fig. 5I).

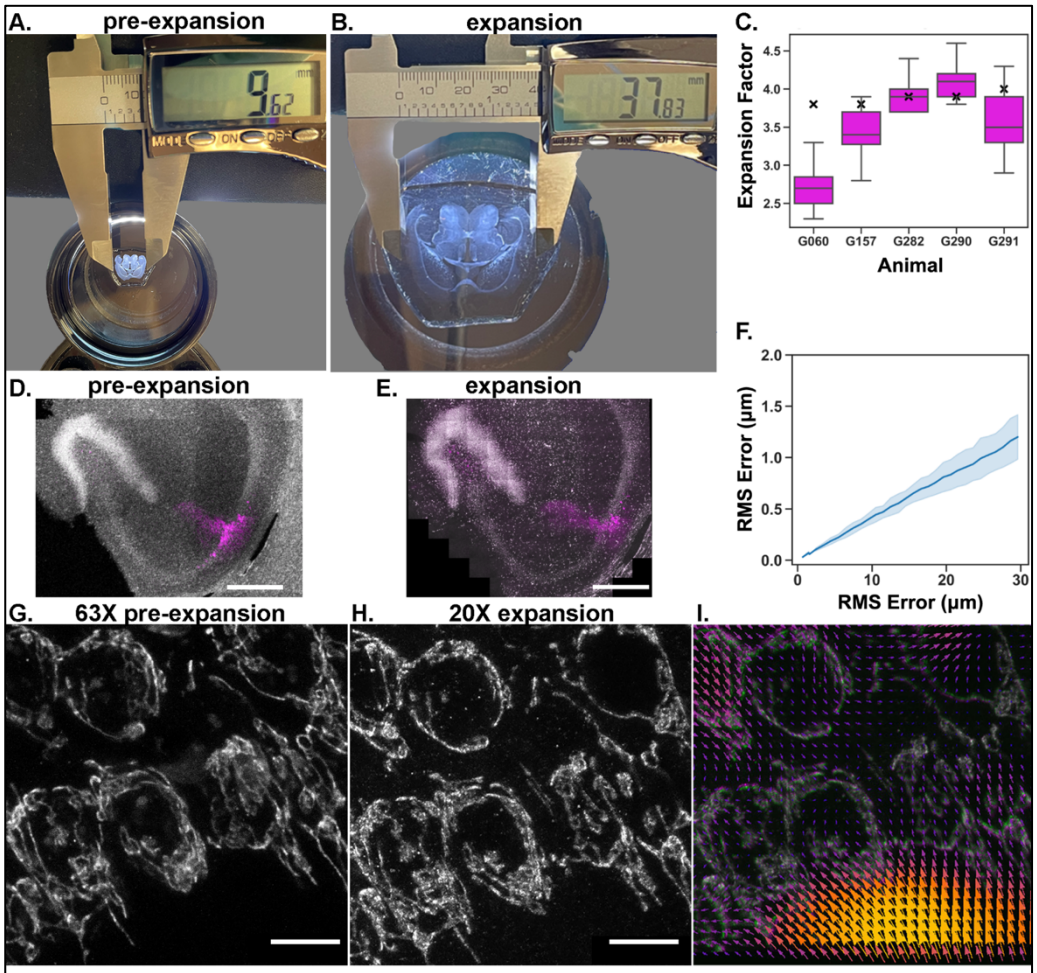

Figure 6: Minimal distortion of tissue or subcellular structures after ProExM
A-B) Representative hydrogels from pre-expanded (**A**) and expanded (**B**) horizontal brain sections after 8-hour digestion with Proteinase K.
C) Micro and macro expansion factors from 5 mice. Box plots show the calculated cell body micro expansion factors (see methods) and X denotes the macro expansion factor of the tissue for each hydrogel as measured in B.
D-E) Representative confocal images of DAPI positive nuclei (grey) and EGFP positive CA2 neurons (magenta) in pre-expanded (5X) and expanded (10X) hippocampus after 8-hour digestion with Proteinase K.
F) Root mean square (RMS) error plot calculated from N=3 gels from 3 mice.
G-I) Representative confocal images of GOLGA5 (grey) immunostaining preExM in 63X unexpanded (**G**) and 20X expanded (**H**) CA2 neurons after 8-hour digestion with Proteinase K. The resulting vector plot (**I**) from b-spline image registration. Arrows indicate the direction and magnitude of the transformation required to align the expanded image to the pre-expanded image.

196 *Subcellular structures in the tissue are minimally distorted after expansion with proExM.*
197 To confirm the IHC-pre-ExM protocol with 8 hours proteinase K digestion reliably maintains
198 macro and micro tissue structure, we measured the macro expansion of the whole tissue section
199 (Fig. 6AB) and the micro expansion of individual cells for 5 different animals (Fig. 6C). The
200 average macro expansion factor was 3.88 and the average micro expansion was 3.33. Example
201 tile images of the same tissue before and after expansion are shown in Fig. 6DE. To quantify the
202 amount of distortion, we performed a root mean squares (RMS) analysis on three sets of
203 GOLGA5 images of the same field of view before and after proExM, as described by Chozinski
204 et. al[1]. The post-ExM image (Fig. 6H) was registered to the preExM image (Fig. 6G) in two
205 steps, with a rigid and then a non-rigid B-spline registration in Elastix. A vector field map was
206 generated (Fig. 6I) and RMS was calculated with code provided by Chozinski et. al. (see
207 Methods). Over a length of 10 µm, the average RMS error across the three animals was 0.2 µm,
208 which is a 2% error. This is in line with previous publications[10] and demonstrates little distortion
209 between the pre-ExM images and the post-ExM images.
210

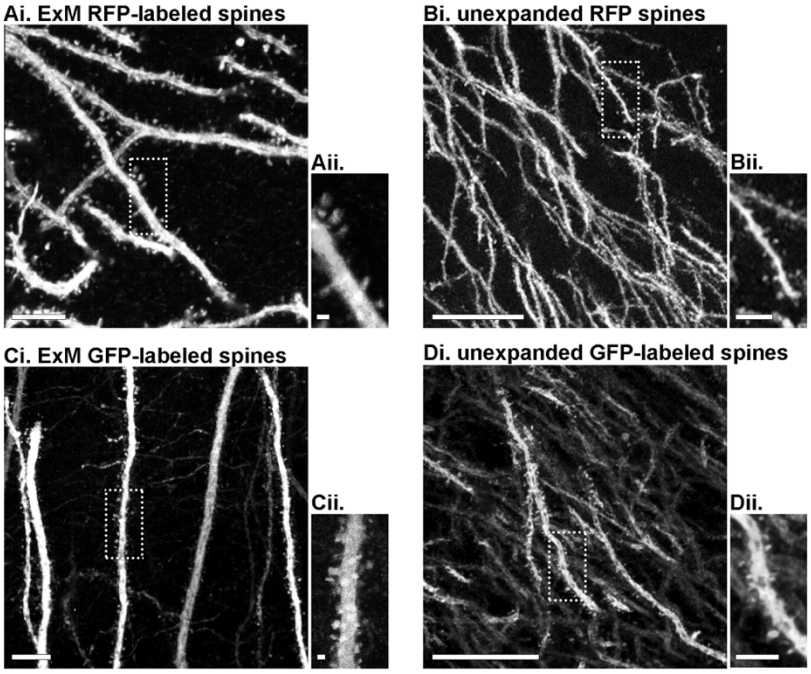

Figure 7: Resolving dendritic spines with ExM.
A) 20X with 3X zoom max-projection image (i) of a section immunostained for RFP pre-ExM with overnight Proteinase K digestion. This mouse received 2 tamoxifen injections. (ii) Insets are 2X zoomed images of the dotted box in (i). All images were acquired with parameters optimal per condition. Brightness and contrast were adjusted per condition across the entire image.
B) 40X with 2X zoom max-projection image of an unexpanded tdTomato section. This mouse received 2 tamoxifen injections.
C) 20X with 2X zoom max-projection image of a section immunostained for GFP pre-ExM with overnight Proteinase K digestion.
D) 40X with 2X zoom max-projection image from an unexpanded section immunostained for GFP. Note the increased background labeling and density of dendritic branches in the unexpanded images, making dendrites more difficult to trace compared with expanded images.
Scale bars: 25µm (**Ai**, **Bi**, **Ci**, **Di**) and 5µm (**Aii**, **Bii**, **Cii**, **Dii**).
211

212 *Dendritic spines are best resolved in expanded GFP or RFP-immunolabeled tissue*
213 In addition to resolving subcellular organelles such as mitochondria and Golgi apparatus, the
214 ability to resolve fine dendritic structures such as spines allows us to address questions about
215 function and plasticity at synapses. Thus, we set out to find the optimal combination of ExM
216 conditions for subcellular organelles and reporter antibodies to resolve dendritic spines in EGFP
217 and tdTomato reporter mice. Table 3 compares spines in unexpanded and expanded tissue, with
218 or without immunolabeling for the reporter protein, and with or without antigen retrieval by
219 boiling or citrate. Expanded samples were immunostained pre-ExM (if at all) and digested
220 overnight with proteinase K, as described in the methods. To boost the signal of the reporter
221 protein, we tested two antibodies against each EGFP and tdTomato reporters (anti-GFP and anti-
222 RFP, respectively). The ability to resolve dendritic spines in each condition was qualitatively
223 assessed by multiple investigators (not blinded to condition), and indicated by the number of + in
224 the table (from + to ++++). A greater number of + indicates better discrimination of spines and
225 "-" indicates dendritic spines could not be resolved for a given condition. Some conditions in the
226 table have yet to be tested as indicated where applicable.
227
228 Figure 7 shows representative images of dendritic spines for each of the four conditions tested.
229 We saw the best resolution of spines in expanded tdTomato+ tissue that was stained with the
230 rabbit anti-RFP without any antigen retrieval (Fig. 7A; "Am2-icre;tdTomato/RFP-rabbit" in
231 Table 3). We noted that the chicken RFP antibody did not label spines as well as the rabbit RFP
232 antibody ("Am2-icre;tdTomato/RFP-chicken", Table 3), indicating that not all reporter
233 antibodies are equal when it comes to labeling spines. In general, spines were easier to resolve
234 with proExM in tdTomato reporter mice (top panel) compared to EGFP reporter mice (bottom
235 panel). The reason is likely multifactorial: a combination of a better performing RFP antibody, a
236 difference in fluorescence retention between tdTomato and EGFP after proExM[2], and a
237 difference in fluorescence retention between their secondary antibodies (Alexa546 and
238 Alexa488, respectively) after proExM[2].We find CA2 spines are difficult to visualize in either
239 mouse strain without prior immunolabeling. Thus, we do not believe mouse strain differences
240 account for the differences in spine labeling after proExM. Compared to unexpanded tissue with
241 the same IHC conditions, the proExM protocol increases the resolution of spines by increasing
242 their physical size and separation from nearby dendritic branches and reducing background
243 fluorescence and/or light scattering[11] to enable spine morphometric analyses on individually
244 traced neurons.
245
246 **DISCUSSION**
247 ProExM is a powerful tool that increases the resolution of conventional fluorescence microscopy
248 to ~70 nm and can be performed with tools available in a standard molecular biology
249 laboratory[10,12]. Because a fully expanded hydrogel is mostly water, the optically clear sample is
250 well suited to resolve densely packed organelles and tissues. However, the digestion and
251 expansion process greatly reduces fluorescence retention making it necessary to optimize ExM
252 conditions per sample for specific end goals. Here we described a proExM workflow optimized

253 for resolving subcellular organelles (mitochondria and the Golgi apparatus) and spines in fixed
254 mouse brain tissue. We reliably found that immunostaining before proExM (IHC-pre-ExM) and
255 using a proteinase K based digestion for 8 hours resulted in the best fluorescence signal to
256 resolve subcellular organelles while maintaining sufficient reporter labeling to visualize spines
257 and trace individual neurons. With these methods, we were able to more accurately quantify
258 mitochondria size and number and better visualize Golgi ultrastructure in reconstructed CA2 cell
259 bodies in the hippocampus.
260
261 Several groups have optimized expansion protocols to visualize subcellular organelles across
262 different sample types, including various cell lines[1,5,8,13–16], rat liver[17], clinical specimens[18],
263 fungi[6,19], songbird[20] and drosophila[21,22]. Others have used ExM to visualize subcellular
264 structures, including mitochondria[1,2,23–25] and/or spines[2,20,23] in brain tissue, but few have
265 systematically analyzed how fluorescence intensities and expansion factors compare across
266 protocols or with unexpanded measurements. This is critically important as several groups have
267 noted discrepancies in micro versus macro expansion factors in other sample types[7,14,17,26–28],
268 including dissimilarities in expansion factors of different subcellular organelles[14] or of
269 subcellular organelles across neighboring cells and tissues[17]. Others, however, have reported
270 minimal to no differences in micro vs macro expansion factors[6,19]. In our measurements, we
271 found discrepancies between the micro and macro-expansion factors. On average, the 8-hour
272 proteinase K digestion produced a micro expansion factor of 3.33 and a macro expansion factor
273 of 3.88 (Fig. 6C). Interestingly, the macro expansion factor was relatively insensitive to digestion
274 time past 2 hours, while the micro factor continued to increase (Fig. 1F). Our average micro
275 expansion factors are lower than the commonly reported 4-4.5X macro expansion factor for
276 proExM, which is consistent with other reports using micro expansion factor measurements[14,15]
277 (but see also ref[26]), reinforcing the notion that each sample type needs to be independently
278 optimized and validated for ExM.

279 To determine the optimal digestion time for fluorescence retention in fixed brain sections, we
280 performed a digestion time course and found the greatest drop in fluorescence after the overnight
281 digestion. There was no significant drop in fluorescence between 2, 4 or 8 hours of digestion.
282 However, there was a significant increase in expansion factor during this time period. Expansion
283 factor begins to plateau after 8 hours of digestion, and while there is a slight increase in
284 expansion factor in the overnight condition it is not statistically significant. Therefore, under the
285 conditions used here, a digestion time of 8 hours is ideal for achieving a robust expansion (~3X)
286 without further loss of fluorescence seen with overnight digestion. At all digestion time points,
287 the expansion factor did not systematically vary by depth, indicating that 2 hours in proteinase K
288 is sufficient for uniform penetration and isotropic expansion in the Z dimension of 40 micron
289 brain sections, as previously reported for thicker sections and longer digestion times[10].

290 In regards to labeling subcellular organelles in fixed brain sections, we were able to visualize
291 expanded mitochondria with a COX4 antibody and expanded Golgi apparatus with a GOLGA5

292 antibody, using either the proteinase K digestion or the mild autoclave digestion. In our hands,
293 the IHC-pre ExM with proteinase K digestion outperformed the other conditions based on
294 fluorescence signal retention for both immunostained organelles and reporter proteins. While
295 EGFP and tdTomato have been reported to have different percent fluorescence retention after
296 ExM[2], they perform comparably when antibody-labeled prior to ExM, as recently reported in
297 cultured cells[29]. They also retain more fluorescence with proteinase K digestion compared with
298 autoclave digestion. However, if the goal is only to visualize mitochondria, the mild autoclave
299 digestion with IHC-post ExM also produced good COX4 staining, as seen for other mitochondria
300 immunostains, like TOMM20[2]. The GOLGA5 antibody performed decently using IHC-pre ExM
301 and autoclave digestion, which the COX4 antibody did not, likely due to COX4 immunostaining
302 requiring antigen retrieval. Neither antibody performed well with IHC-post ExM and proteinase
303 K digestion. It is important to note that conducting immunostaining prior to proExM introduces
304 small positional errors due to linking the fluorophores into the gel. Immunostaining targets with
305 primary and secondary antibodies imposes a linkage error of ~17.5 nm[30,31]. This can cause a
306 localization error between a protein of interest and its fluorophore in an expanded state, however,
307 the relative distance of the fluorophore to the epitope stays unchanged. This is in contrast to post-
308 ExM labeling that leads to a relative smaller antibody size[6].

309 Despite diminished fluorescence, ExM afforded better resolution for quantification of
310 subcellular organelles compared to unexpanded organelles. We quantified the number and size of
311 expanded mitochondria and found that the expanded mitochondria were smaller and more
312 numerous than unexpanded mitochondria. This presumably is indicative of tightly packed
313 mitochondria in the unexpanded samples being lumped together that can be separately resolved
314 with expansion. Here, we normalized subcellular measurements (i.e. mitochondria size) to within
315 cell nuclear and cytoplasmic areas. Another study found discrepancies in cell soma vs nuclear
316 expansion factors[17], but here the ratio of nuclear area to cytoplasmic area remained constant
317 between unexpanded and expanded states, indicating isotropic expansion, perhaps due to our
318 longer digestion times.

319 The fine details of the Golgi cisternae were also better resolved after expansion, whereas
320 without expansion the Golgi were smoothened and much of the details lost. For the goal of
321 visualizing reporter-labeled dendritic spines, we found that the addition of IHC-pre ExM was
322 necessary for the resolution of both EGFP+ and tdTomato+ spines. Dendritic spines were best
323 resolved in IHC-pre ExM with proteinase K digestion with either GFP or RFP antibodies. The
324 ability to label dendritic spines in ExM was antibody dependent, with some antibodies against
325 the same reporter faring better than others under the same IHC conditions.

326 Our lab has begun applying the described proExM methods to answer open questions
327 involving subcellular organelles in neurons. One such open question is whether there is Golgi
328 present in dendrites, or if the Golgi is limited to neuronal cell bodies. It is known that local
329 translation of RNA occurs in dendrites[32]; however, there is conflicting evidence of the existence

330 of Golgi apparatus in the dendrites , which would normally process newly transcribed membrane
331 bound proteins. Using combined GOLGA5-labeling of Golgi apparatus and reporter neuron
332 labeling with the proExM protocol described here, we do not detect GOLGA5 staining outside
333 the cell soma or very proximal dendrites, consistent with reports that canonical Golgi markers
334 are retained in the soma and not present in distal dendrites[25,34,35].
335
336 *Considerations for subcellular imaging of expanded samples*
337 The benefits of expansion come at several costs, including diminished signal concentration,
338 hydrogel mechanical integrity and movement, and increased imaging volume and time[5]. Here we
339 comment on the proposed workarounds for these issues that have or have not worked well for
340 subcellular imaging of expanded brain sections.
341
342 Expansion microscopy substantially increases the thickness of a sample, which limits its ability
343 to be imaged with standard high magnification microscope objectives with limited working
344 distances. It can be expected that the gel thickness will be equivalent to 4-fold the depth of the
345 gelation chamber. Further, keeping the tissue in plane during gel chamber assembly is difficult,
346 often resulting in increased sample z-distance. Minimizing tissue thickness (40 microns versus
347 100 microns) and using a single coverslip for the gelation chamber helped minimize gel
348 thickness without sacrificing ability to reconstruct neurons. However, in our hands, digestion
349 time need to be decreased to 4 hours when using a single coverslip versus 8 hours for two
350 coverslips as optimized here.
351
352 Loss of fluorescence due to the digestion of antibodies or epitopes and dilution of fluorescent
353 molecules per unit volume can result in low contrast samples not suitable for high resolution
354 imaging even with overexpressed fluorescent reporter proteins. We found that performing IHC
355 beforehand and limiting the proteinase K digestion to 8 hours largely negated this issue. When
356 the fluorescence signal is insufficient, imaging in low concentrations of PBS (0.5X PBS instead
357 of 0.0001X PBS or water) substantially improved the contrast by increasing the concentration of
358 fluorescent molecules per area. This will decrease the expansion factor, but in our hands, even a
359 2-3-fold expansion in optically clear tissue produces better resolved images of subcellular
360 structures than unexpanded tissue.
361
362 Hydrogel movement during imaging is another common issue. Because gels expand 4-fold in x,
363 y and z compared with unexpanded brain sections, tile scans are required to reconstruct entire
364 neurons even at 10x (see Fig. 2Fii for a 10x single field of view of expanded neurons). Tile
365 scanning increases the length of time required to image a gel and thus worsens gel shift. Gel shift
366 was most noticeable while imaging on an upright microscope equipped with a water immersion
367 lens, since the gel can easily shift when submerged. Gel shift was less noticeable when imaging
368 either on an inverted scope or on an upright scope with air objectives (if the gel was dried for 30
369 minutes to adhere to the glass bottom plate), but these options negatively impact objective
370 working distance or resolution, respectively. To minimize gel shift during upright imaging with a

371 water dipping lens, we applied the following techniques to stabilize the gel in the imaging
372 chamber (50 mm WillCo Well). Following full expansion in water, we surrounded the gel with
373 2% agarose in the imaging chamber. This noticeably reduced gel movement during acquisition of
374 single images but shift was still detected during longer tile scans. We also tested re-embedding
375 the gelated sample in an unexpandable gel and covalently linking it to the glass imaging dish[2].
376 This completely eliminated movement of the gel and allowed us to take long tile scans on an
377 upright or inverted microscope. Unexpectedly, however, this also seemed to dampen the
378 fluorescence signal, which was irreversible.
379
380 **Table 1: Digestion time course.** Table showing mean expansion factor and fluorescence
381 intensities (FI) for each digestion time point and the unexpanded control. Also included is the
382 average background fluorescence intensity ("BG FI"), the normalized $\log_2$ transformed
383 fluorescence, and the number of cells ("N Cells") for each digestion condition.

Digest Time	Exp Factor	Mean FI	BG FI	$\log_2$ Norm FI	N Cells
no ExM	1.0 (±0.02)	69.0 (±5.39)	7.24 (±0.63)	5.795 (±0.12)	31
2 hour	2.6 (±0.08)	32.91 (±1.93)	3.56 (±0.4)	4.78 (±0.10)	29
4 hour	2.6 (±0.06)	42.79 (±4.77)	4.21 (±0.24)	5.024 (±0.14)	33
8 hour	3.0 (±0.08)	32.43 (±2.43)	2.34 (±0.01)	4.742 (±0.13)	35
overnight	3.2 (±0.05)	22.84 (±2.72)	2.28 (±0.03)	4.025 (±0.18)	31

384
385
386 **Table 2: Antibodies and conditions.** Table showing primary and secondary antibody conditions
387 used for expansion microscopy.

Primary Antibody	Host	Clonality	Supplier	Catalogue #	Antigen retrieval	Concentration	Incubation
GFP	Chicken	Polyclonal IgY	Abcam	ab13970	Not Required	1:500	72+ hrs at RT
GFP Booster Atto 488	Alpaca	Monoclonal VHH	Chromotek	gba488-100	Not Required	1:200	72+ hrs at RT
RFP	Rabbit	Polyclonal IgG	Rockland	600-401-379	Not Required	1:500	72+ hrs at RT
RFP	Chicken	Polyclonal IgY	Rockland	600-901-379	Not Required	1:250	72+hrs at RT
GOLGA5/Golgin-84	Rabbit	Polyclonal IgG	Abcam	ab224040	Not Required	1:500	72+ hrs at RT
COX4	Rabbit	Polyclonal IgG	Synaptic Systems	298 003	5 min at 100C	1:500	72+hrs at RT
ERGIC-53/P58	Rabbit	Polyclonal IgG	Sigma Aldrich	E1031	Citrate at 80C	1:600	72+ hrs at RT
ST3GAL5	Rabbit	Polyclonal IgG	Sigma Aldrich	AV46358	Citrate at 80C	1:250	72+ hrs at RT
MCU	Rabbit	Polyclonal IgG	Sigma Aldrich	HPA016480	5 min at 100C	1:500	72+ hrs at RT

Secondary Antibody							
Goat anti Mouse IgG (H+L) Alexa 488	Goat	Polyclonal IgG	Invitrogen	A11029	NA	1:500	48+ hrs at RT
Goat anti Mouse IgG (H+L) Alexa 546	Goat	Polyclonal IgG	Invitrogen	A11030	NA	1:500	48+ hrs at RT
Goat anti Rabbit IgG (H+L) Alexa 488	Goat	Polyclonal IgG	Invitrogen	A11034	NA	1:500	48+ hrs at RT
Goat anti Rabbit IgG (H+L) Alexa 546	Goat	Polyclonal IgG	Invitrogen	A11035	NA	1:500	48+ hrs at RT
Goat anti Chicken IgY (H+L) Alexa 488	Goat	Polyclonal IgY	Invitrogen	A11039	NA	1:500	48+ hrs at RT
Goat anti Chicken IgY (H+L) Alexa 546	Goat	Polyclonal IgY	Invitrogen	A11040	NA	1:500	48+ hrs at RT

388

389 **Table 3: Detection of reporter labeled spines**

Tissue/Antibody	ExM (protK)	IHC (pre-ExM)	Spines
Am2-GFP	unexpanded	no IHC	+
		ag-no IHC	-
	expanded	no IHC	-
		ag-no IHC	-
Am2-GFP/GFP-chicken	unexpanded	IHC	++
		ag-IHC	+
	expanded	IHC	+++
		ag-IHC	++
Am2-GFP/GFP booster-alpaca	unexpanded	IHC	+
		ag-IHC	-
	expanded	IHC	-
		ag-IHC	nt
Am2-icre;tdTomato	unexpanded	no IHC	+
		ag-no IHC	+
	expanded	no IHC	-
		ag-no IHC	nt
Am2-icre;tdTomato/RFP-chicken	unexpanded	IHC	+++
		ag-IHC	+
	expanded	IHC	++
		ag-IHC	+

Am2-icre;tdTomato/RFP-rabbit	unexpanded	IHC	++++
		ag-IHC	nt
	expanded	IHC	++++
		ag-IHC	nt
- not detected; + rare SLM only; ++ OK; +++ Good; ++++ Excellent; nt Not tested			

390
391

392 **METHODS**
393
394 **Animals**
395 Adult male and female Amigo2-EGFP (RRID:MMRRC 033018-UCD, bred for at least 10
396 generations onto C57BL/6J background) or Amigo2-icreERT2;RosaTdTomato transgenic mice
397 were used. Amigo2-icreERT2;RosaTdTomato mice were generated by crossing Amigo2-
398 icreERT2 mice[36] to Ai14 mice (Jax #007914). Amigo2-icreER;ROSA-TdTomato mice were
399 given 2 or 3 daily intraperitoneal injections of tamoxifen (Sigma T5648, 100mg/kg freshly
400 dissolved daily in 100% ethanol then diluted 10-fold in corn oil and heated at 60C for 1 hour
401 until in solution). Mice were group-housed under a 12:12 light/dark cycle with access to food
402 and water *ad libitum*. All procedures were approved by the Animal Care and Use Committee of
403 Virginia Tech.
404
405 **Immunofluorescence**
406 Mice were anesthetized with 150mg/kg fatal plus solution and perfused with ice-cold 4%
407 paraformaldehyde. Amigo2-icreERT2;RosaTdTomato mice were perfused one week post
408 tamoxifen injections. Brains were dissected and post-fixed for at least 24 hours before sectioning
409 40 µm thick sections in the horizontal plane on a vibratome (Leica VT1000S). Sections to be
410 stained with COX4 underwent antigen retrieval by boiling free floating sections in 1.7ml tubes
411 for 3 min in nanopure water. All sections were washed in PBS and blocked for at least 1 hour in
412 5% Normal Goat Serum (NGS)/0.3% Triton-100x. See Table 3 for primary and secondary
413 antibodies and conditions. Antibodies were diluted in blocking solution and sections were
414 incubated for 72+ hours at room temperature (RT). After several rinses in PBS-T (0.3% Triton-
415 100x), sections were incubated in secondary antibodies for 48 hours at RT. Prior to imaging,
416 unexpanded sections were washed in PBS-T and mounted under Vectashield fluorescence media
417 with 4′,6-diamidino-2-phenylindole (DAPI) (Vector Laboratories).
418
419 **Protein expansion microscopy solution preparation**
420 Solutions were prepared as described by Asano et. al 2018[3]. Anchoring stock solution was
421 prepared by dissolving Acryloyl-X, SE (ThermoFisher A20770) in DMSO (1:100 w/v) and
422 stored at -20C. Monomer solution components were prepared by dissolving Sodium Acrylate in
423 npH20 (33% w/v, Sigma 408220), Acrylamide in npH20 (50% w/v, Sigma A9099), N, N'-
424 Methylenebisacylamide in npH20 (2% w/v, Sigma M7279). Monomer working solution was
425 prepared by adding 2.25mL of 33% SA solution (8.6% w/v), 0.5 mL of 50% Acrylamide
426 solution (2.5% w/v), 0.75 mL of 2% N,N-Methylenebisacrylamide solution (0.15% w/v), 4 mL
427 of 5M NaCl (11.7% w/v), and 1 mL of 10X PBS. Inhibitor stock was prepared by dissolving 4-
428 Hydroxy-TEMPO (0.5% w/v, Sigma 176141) in npH2O and initiator stock was made by
429 dissolving Ammonium persulfate in npH2O (10% w/v, Sigma 248614). Accelerator solution was
430 prepared by diluting TEMED in npH2O (10% v/v, Sigma T7024) immediately before use. All
431 solutions except the TEMED accelerator were prepared before use and stored at -20C.

432
433 **Protein expansion microscopy**
434 4X protein expansion microscopy (proExM) was carried out on horizontal mouse brain sections
435 containing dorsal hippocampus as described in Asano et al 2018[3]. Sections were incubated
436 overnight in Acryloyl-X stock/PBS (1:100, ThermoFisher, A20770) at RT in the dark. Following
437 incubation, the slices were washed twice with PBS for 15 minutes each at RT. The gelation
438 solution was prepared by adding 384 uL of monomer solution, 8 uL 4-Hydroxy-TEMPO
439 inhibitor (1:200 w/v, Sigma Aldrich, 176141), 8uL TEMED accelerator (10% v/v, Sigma
440 Aldrich, T7024), and lastly 8uL of APS initiator (10% w/v, Sigma Aldrich, 248614) for each
441 section. Sections were then incubated in the gelation solution for 30-45 minutes at 4C in the
442 dark. Gelated sections were placed on gelation chambers constructed from microscope slides
443 with coverslips as spacers. Our gelation chambers produce gels with the thickness of two type
444 No. 1.5 coverslips (~0.3mm thick). The chambers were filled with gelation solution and allowed
445 to incubate at 37 C for 2 hours in a humidified container. Following gelation incubation, the
446 gelation chamber was deconstructed to uncover the gelated brain section. To remove the gel
447 from the chamber, digestion solution without proteinase K was applied and a coverslip was used
448 to gently remove the sample. Digestion solution containing proteinase K (8U/mL, New England
449 BioLabs, P8107S) was applied to gels and allowed to digest for 2-16 hours (see Results) at room
450 temperature. Upon completion of digestion, gels were stained with DAPI (Sigma Aldrich,
451 D9542, 1:10,000 in PBS) for 10 minutes at room temperature with shaking. The gels were then
452 washed twice for 10 minutes with npH2O to remove excess DAPI and fully expand the gel.
453
454 *Stabilizing ExM Gels with Agarose*
455 To prevent movement during imaging, gels were fully expanded in water or 0.001X PBS in
456 WillCo wells (HBSB-5040) and reversibly immobilized by applying liquid 2% agarose around
457 and on top of the gel (in areas not containing tissue). Following application, the gel embedded
458 with agarose was placed at 4C for at least 15 minutes to allow the agarose to fully solidify prior
459 to imaging.
460
461 *Re-embedding and Linking Gels to Imaging Dish*
462 Re-embedding and covalently linking gels to a WillCo well allowed long-term imaging without
463 gel shifting as described by Tillberg et al 2016[2]. First, the gel was completely expanded in water
464 and then incubated in a non-expanding re-embedding solution (3% w/v acrylamide, 0.15% w/v
465 N,N-methylenebisacylamide, 0.05% w/v APS, 0.05% w/v TEMED, and 5mM Tris). The gels
466 were incubated with shaking at room temperature for 20 minutes. The gel was then transferred to
467 a Bind-Silane treated WillCo Well plate and covered with a coverslip. Fresh re-embedding
468 solution was then lightly applied surrounding the sample, which was then incubated at 37C for
469 1.5-2hrs without shaking. Once the re-embedding solution gelated, the coverslip was removed
470 from the covalently linked gel and could be imaged.
471

472 *Bind Silane Treatment of Imaging Dishes*
473 Immediately before use, imaging dishes were treated with a bind silane solution as described by
474 Tillberg et al 2016[2]. Before bind silane treatment, imaging dishes were briefly washed with
475 npH2O, 100% Ethanol, and then allowed to dry. Bind silane solution (80% v/v EtOH, 2% v/v
476 acetic acid, 0.05% v/v Bind-Silane) was then applied with shaking for 5 minutes. The dish was
477 then washed with 100% EtOH and allowed to dry before usage.
478
479 *Digestion Time Course Experiment*
480 To assess the effect of digestion time on tissue expansion and fluorescence retention, we ran a
481 digestion time course experiment by varying the amount of time the ExM gels were in digestion
482 solution-- either 2 hours, 4 hours, 8 hours or 16 hours (overnight). The brains of two Amigo2-
483 EGFP mice (One male and one female, 21-23 weeks old) were processed as above. During a
484 pilot run, we noted that samples with digestion > 2 hours lost the majority of EGFP fluorescence,
485 making it impossible to acquire images with identical parameters for direct comparison.
486 Therefore, to boost the EGFP signal, approximately ten sections per brain (two sections per
487 condition per mouse) were first immunostained in a 24-well plate as described in the
488 immunohistochemistry methods, with a primary chicken antibody against EGFP (Abcam,
489 ab13970; 1:500 concentration) at RT for 3 days, followed by a secondary antibody (Invitrogen
490 Alexa-488, A11039; 1:500 concentration) incubation for 48 hours. As a control, a few sections
491 were set aside after immunostaining to mount on slides without expanding.
492
493 Sections processed for ExM were anchored in Acryloyl-X overnight, washed twice with 1X PBS
494 and incubated in gelation solution for 30 min at 4C the following day (see "Protein Expansion
495 Methods" for more detail). The gels were incubated in a humid environment at 37C for 2 hours
496 to set, and then carefully removed from the chamber and placed in a digestion solution with 8
497 U/mL of proteinase K (New England Bio, Cat # P8107S) for the designated period of time. All
498 gels in this experiment were digested on a shaker at room temperature. At the end of the
499 digestion time, the digestion solution was replaced with 1X PBS several times to wash the gels.
500 Gels were stored in 1X PBS in the dark at 4C until imaging, at which point the PBS was replaced
501 with npH2O to fully expand the gels. Gels were imaged at 10X (EC-Plan-Neofluar lens; 10x; 0.3
502 NA; 5.2mm WD) taking 10μm steps for distance on a Zeiss 710 confocal microscope with the
503 same image acquisition parameters, as described in more detail under "image acquisition".
504
505 *Digestion Time Course Analysis*
506 The ExM images from the time course experiment were analyzed with the image processing
507 program Fiji (v.+03..30, NIH). Before analysis, images were flattened across the Z dimension
508 with the *"Z Project"* function to get an idea of how many GFP positive cells were present. This
509 flattened image was only used for the selection of cells. Cells were excluded from analysis if
510 they met any of the following criteria: 1) Incomplete cell (i.e. on the image border); 2) Any cell
511 overlapping in Z with a cell already analyzed; 3) Cells with an ambiguous border or that were

512 difficult to differentiate. Given these exclusion criteria, an average of 32 cells were analyzed for
513 each time point across both animals. For some time points, cells were included from multiple
514 hippocampal sections from the same animal.
515
516 For the fluorescence analysis, each cell body meeting the inclusion criteria was manually traced
517 with the freehand selection tool in a single z section at the widest point of the cell. Once the cells
518 were traced, the *"measure"* tool in Fiji was used to measure the mean intensity and the area
519 within each individual cell ROI. To subtract background signal, one cell ROI was selected (at
520 random) and moved to a location without EGFP signal and the background mean intensity was
521 measured. The background mean intensity value was subtracted from the mean fluorescence
522 intensity of each cell from the same image, resulting in a normalized mean fluorescence. The
523 area of the cell body ROIs were used to calculate expansion factor by comparing it to the average
524 area of 37 unexpanded cell bodies, which was calculated to be 300 μm^2. To calculate the linear
525 expansion factor for each cell, we used the below formula:
526

$$\textit{Linear Expansion Factor} = \frac{\sqrt{(cell\ area)}}{\sqrt{(avg\ non\ expanded\ cell\ area)}}$$

527
528
529 A total of 159 cells were included in the analyses (average of 32 +/- 4 cells per time point from
530 two brains). The mean fluorescence and expansion factor measurements were imported into
531 Python (v 3.7, installed with the Anaconda distribution), where the average mean fluorescence
532 and average linear expansion factor were calculated for each time point, including the
533 unexpanded control (see Fig. 2). The mean fluorescence data was not normally distributed
534 (Shapiro-Wilk test for normality; $p < 0.0001$), so the mean fluorescence data was $\log_2$
535 transformed and 11 cell means were removed as outliers, pre-defined as two standard deviations
536 from the mean. These same outliers were also removed from the expansion factor data; however,
537 because this data was normally distributed (Shapiro-Wilk; $p = 0.235$), it was not transformed.
538 One-way ANOVAs were run using an ordinary least squares model with the StatsModels
539 package (ols, ANOVA_lm, statsmodels v0.11.1) comparing fluorescence intensity and linear
540 expansion factors across digestion time points. After overall significance was reached, pairwise
541 post-hoc Tukey's multiple comparison tests (pairwise_tukeyhsd, statsmodels v0.11.1) were
542 performed to determine which digestion time points were significantly different (see Fig. 2D).
543
544 *Analysis of Expanded and Unexpanded Mitochondria*
545 To determine if the proExM protocol affects our ability to resolve and quantify mitochondria, we
546 analyzed the number and size of expanded mitochondria compared to unexpanded mitochondria.
547 Tissue from an adult male EGFP reporter mouse was immunostained with COX4 to label
548 mitochondria and expanded using our optimized ExM protocol with overnight digestion in
549 proteinase K (see Expansion Microscopy methods). An adult male tdTomato reporter mouse was
550 similarly processed and immunostained with COX4 but not expanded. Confocal images were

551 taken of both samples for image analysis in FIJI. Note that the COX4 signal was imaged in
552 different color channels for the expanded and unexpanded samples (546nm vs 488nm,
553 respectively).
554
555 Confocal images were imported into Fiji and converted to 8-bit for the analysis. An intensity
556 threshold was chosen separately for each image which best represented the signal in the original
557 image. Using the reporter label as a guide, four cells were analyzed from the expanded sample
558 and five cells from the unexpanded sample. Cells were chosen using the same criteria as for the
559 digestion time course analysis. An ROI for each cell was drawn by fitting an oval to the cell
560 body using the oval selection tool, rotating if necessary, and the signal outside of the cell's ROI
561 was removed for the analysis. The "*nucleus counter"* plug-in from the FIJI "Cookbook"
562 microscopy analysis collection was used to segment mitochondria within the ROI of each cell
563 analyzed. The size threshold used for the expanded sample was adjusted for expansion factor,
564 which was calculated using the ratio of the cell body diameters in the expanded images
565 compared to the unexpanded images. The calculated expansion factor for the expanded images
566 was 3x in the X and Y dimensions-- an expansion factor of 9x in total area.
567
568 Once the mitochondria were properly segmented, FIJI's "*measure"* feature was used to measure
569 the number, area and intensity of each individual mitochondrial ROI. A custom Python code was
570 written to calculate and plot the averages of the mitochondria number, size and total area for the
571 expanded cells and the unexpanded cells. To account for the effect of expansion on size, the area
572 of each mitochondria was divided by the area of the soma to get a normalized mitochondria area.
573 The mitochondrial coverage was calculated by dividing the total summed mitochondrial area in
574 the cell by the area of the cytoplasm (*soma area – nucleus area*) and converting it to a
575 percentage.
576
577 **Image acquisition**
578 Images were acquired on an upright Zeiss 710 or inverted Zeiss 700 confocal microscope
579 equipped with a motorized stage, 488/561/633 laser lines, and 5X/0.16 NA, 10X/0.3NA, 20X/1.0
580 NA water immersion, 20X/0.4 NA air, or 63X/1.4NA lenses. Gels were expanded by washing
581 with 0.001X PBS three times and by incubating overnight at RT in 0.001X PBS. Gels were
582 immobilized in 50mm glass bottom wells (WillCo Wells, HBSB-5040) by applying 2% agarose
583 to the edges of the gels. Gels were then imaged in a fully expanded state in or 0.001X PBS. A
584 subset of images (Fig. 4K-L, Fig. 5G-H) were acquired on an Olympus SpinSR10 spinning disk
585 confocal with a 25X silicone lens. Scale bars are not adjusted for expansion factor unless
586 specifically stated.
587
588 **ExM image processing**
589 Czi files were imported into Fiji, individual channel images were split and adjusted for
590 brightness and contrast equivalently across conditions, then images were viewed with the volume

591 viewer plugin (v. 2.01.2). If images showed considerable shift or too many neurons overlapped, a
592 subset stack was created without the offending Z sections. Mode was set to max-projection and
593 interpolation was set to tricubic smooth with z-aspect and sampling optimized per image
594 (typically 0.5-2.0 for each parameter). Snapshots were taken in the XY plane at 1.0 and 2.0 scale
595 in grayscale and 1D. The resulting snapshot images were imported into Photoshop (v. 21.2) and
596 converted to 300 dpi. Any further brightness and contrast edits done in photoshop were minimal
597 and applied equivalently to all comparable images in the figure.
598
599 **Semi-quantitative histological assessment of ExM protocols**
600 To quantify the brightness and the quality of the staining after expansion with the various ExM
601 protocols tested in Figures 4 and 5, we developed a scoring system similar to what was done by
602 the Boyden lab (Yu et al, 2020, see Fig. 11). The mean fluorescence of the cropped image was
603 measured in Fiji for each condition, for either the COX4 channel (Fig. 4) or the GOLGA5
604 channel (Fig. 5) and the reporter channel (GFP or RFP). We normalized the fluorescence by the
605 brightest image in the set to get a fluorescence scale from 0-1. In addition to fluorescence, we
606 gave each image a quality score from 0-1, which took into account how much noise there was in
607 the image and also how close the observed staining was to the expected staining pattern in non-
608 expanded tissue. The fluorescence and quality scores were averaged together and then multiplied
609 by 100 to get an overall score from 0-100 for the antibody and the reporter for each condition.
610
611 **RMS analyses**
612 Horizontal 40µm GFP+ sections were immunostained for GFP and GOLGA5 as described above
613 for the pre-IHC-ExM with 8 hours proteinase K digestion. The sections were transferred to a
614 glass bottom plate under a drop of 1XPBS and imaged at 5x (0.16 NA) and 63x (1.4 NA). 63X
615 images were taken at the anatomically identifiable CA1-CA2 border. Sections were then washed
616 in PBS and processed for ExM as described above. After gelation, resulting hydrogels were
617 trimmed and the size of the tissue and gel were measured with a caliper. Tissue and gel sizes
618 were also measured following digestion and after expansion in water. All caliper measurements
619 were taken at the widest point of the section.
620
621 Gels were post-stained with DAPI (1:5,000 in water) for 30 minutes and transferred to glass-
622 bottom plates. Gels were then washed in 0.001X PBS overnight. The next day, 10x tile scans of
623 the hippocampus were acquired for each sample. Single 20x images at the CA1-CA2 border
624 were acquired to match the 63x pre-expansion images.
625
626 Images were imported into Fiji and processed to obtain matching ROIs from 63X pre-expansion
627 and 20X post-expansion images. Using GFP labeled gels as landmarks, images were cropped to a
628 square which included only overlapping regions in both pre- and post-expansion images
629 (typically 50 x 50 µm in pre-expansion dimensions). Substacks were created from the cropped
630 ROIs to include only the matching cells. Max-projected ROIs were converted to 16-bit grey-

scale TIFF files. The pre-ExM image was then scaled in X-Y (with Fiji) to match the pixel dimensions of the post-ExM image, which is needed for proper image registration[38]. The processed images were saved as RAW image files and the associated MHD metadata files were manually created for each image. The GOLGA5 channel was analyzed to get the RMS error. The post-ExM image (moving; Fig. 6H) was registered to the pre-ExM image (fixed; Fig. 6G) using Elastix[39], with a rigid and then a non-rigid registration as described previously (Chozinski et al, Chen et al). In the first step, a similarity registration was done to align the post-ExM image to the pre-ExM image without warping. The resulting image was then registered again to the pre-ExM image with the B-spline non-rigid registration. The results of the first rigid registration and the second B-spline registration were imported into the Wolfram analysis notebook provided by Chozinski et al. to generate a vector field map of the distortion between the two images (Fig. 6I).

The transformix command was used in Elastix to apply the B-spline transform to a skeletonized image of the post-ExM image. To skeletonize the image, a median and gaussian filter were both applied and the image was binarized. With the output of transformix, the RMS error was then calculated for points along the skeletonized image in Wolfram. For plotting, length was binned per micron and cut off at 30 microns to match previously published RMS error data. The three biological replicates were averaged together (Fig. 6F).

Statistical analyses

Statistical analyses were done in python (v 3.7) with an alpha of 0.05 considered significant.

Declarations

Ethics approval and consent to participate

All animal use and procedures were approved by the Animal Care and Use Committee of Virginia Tech.

Consent for publication

Not applicable.

Availability of data and materials

Please contact author for data requests.

Funding

Research reported in this publication was supported by the National Institute of Mental Health of the NIH under award R00MH109626 to S.F. and by startup funds provided by Virginia Tech. The funders had no role in the design of the study and collection, analysis, and interpretation of data and in writing the manuscript.

Competing interests

The authors declare that they have no competing interests.

Authors' contributions

Conceptualization, S.F.; Methodology, L.A.C., K.E.P., N.A.S., D.L., S.F.; Formal Analysis, L.A.C., K.E.P., N.A.S., S.F.; Investigation, L.A.C., K.E.P., N.A.S., D.L., S.F.; Writing – Original Draft, L.A.C., K.E.P., S.F.; Writing – Review & Editing, L.A.C., K.E.P., S.F.; Visualization, L.A.C., K.E.P., S.F.; Supervision, S.F.; Funding Acquisition, S.F.

Acknowledgements

We thank the members of the Farris lab, in particular Daniela Gil, for providing feedback and critically reading this manuscript, as well as the Virginia Tech animal care staff for their support.

684 **FIGURE LEGENDS**
685
686 **Fig. 1: ExM workflow for visualizing subcellular organelles in fixed brain tissue.**
687 Schematic of immunostaining and proExM workflows tested to optimize visualization of
688 organelles in genetically-labeled neurons.
689
690 **Fig. 2: The effect of proteinase K digestion time on fluorescence intensity and expansion**
691 **factor.**
692 **A)** Representative single z-section images of unexpanded (i) and expanded GFP+ CA2 neurons
693 after 2-hour (ii), 4-hour (iii), 8-hour (iv), or overnight (v) digestion with proteinase K. Image
694 acquisition parameters were identical for each condition, except for the unexpanded condition.
695 **B)** GFP fluorescence intensity measured in the cell soma after the different digestion times.
696 Fluorescence was corrected for background and $\log_2$ transformed. Line represents the median.
697 Digestion time had a significant effect on GFP fluorescence (one-way ANOVA; F-stat: 20.96, p-
698 value: 8.17E-14, 32 ± 4 cells per time point from two animals, 159 total cells).
699 **C)** Expansion factor of the expanded cell somas in **B**. Expansion factors were calculated using
700 cell soma areas relative to the average unexpanded cell soma area. Line represents the median.
701 Digestion time had a significant effect on expansion factor (one-way ANOVA; F-stat: 21.07, p-
702 value: 4.26E-11).
703 **D)** Matrix of p-values visualizing the results of pairwise Tukey's post hoc tests comparing mean
704 fluorescence (upper diagonal) or expansion factor (lower diagonal) at each digestion time point.
705 Matrix is color coded by p-value (red = significant; grey = not significant; α=0.05).
706 **E)** Effect of digestion time on fluorescence intensity (cyan; left axis) and expansion factor
707 (orange; right axis). Plot shows the mean and 95% confidence intervals from **B** and **C**.
708 G) Unexpanded (i) and overnight expanded (ii) max-projection 10X confocal images of GFP+
709 CA2 cells. Images are the same as in A(i) and (v). Imaging parameters were optimized separately
710 to obtain the best image of both.
711 **F)** Unexpanded (i) and overnight expanded (ii) max-projection 10X confocal images of GFP+
712 CA2 cells. Images are the same as in **A**(i) and (v). Imaging parameters were optimized separately
713 to obtain the best image of both.
714 Scale bars = (**A**, **F**) 50 μm.
715
716 **Fig. 3: No appreciable effect of tissue depth on expansion factor.**
717 **A)** Average cell soma area (in μm^2) by Z section depth for unexpanded control and digestion
718 conditions. Cell soma area was measured in the Z section with the widest soma diameter.
719 Because of the overall increase in depth with expansion, cells were binned by Z section to
720 achieve ~6 bins per time point. N = 32 ± 4 cells per time point.
721 **B)** Background subtracted average cell soma fluorescence by Z section depth. Binning of the
722 data is the same as in A. The data are not $\log_2$ transformed as in Fig. 2.

723 **C)** Representative confocal images of GFP+ CA2 cell somas after 2-hour (left panel) or
724 overnight (right panel) digestion at three Z-section depths. Cell soma size and fluorescence is
725 variable in the Z dimension in unexpanded conditions, which does not appreciably change under
726 difference digestion conditions.
727 Error bars show the standard deviation. Scale bar is 50µm.
728
729 **Fig. 4: ProExM pipeline comparison for visualizing mitochondria.**
730 **A)** 20X Max-projection image of a section immunostained for COX4 (i) and RFP (iii) pre-ExM
731 with autoclave digestion. Images in panels A-D were acquired with identical imaging parameters
732 to directly compare conditions. Brightness and contrast were adjusted to the same extent across
733 the entire image.
734 **B)** 20X Max-projection image of a boiled section immunostained for COX4 (i) and RFP (ii) pre-
735 ExM with overnight proteinase K digestion.
736 **C)** 20X Max-projection image of a section immunostained for COX4 (i) and RFP (ii) post-ExM
737 with autoclave digestion.
738 **D)** 20X Max-projection image of a boiled section immunostained for COX4 (i) and RFP (ii)
739 post-ExM with overnight proteinase K digestion
740 **E)** 40X Max-projection image from a subset of Z sections from a boiled, unexpanded section
741 immunostained for COX4 and RFP. Inset is a single Z section from the indicated representative
742 cell (white asterisk) with mitochondria outlined as quantified in G-I. Imaging parameters were
743 optimized per condition in E-F.
744 **F)** 20X Max-projection image from a subset of Z sections from a boiled section immunostained
745 for COX4 and GFP pre-ExM with overnight proteinase K digestion as in **B.**
746 **G)** The average number of mitochondria per cell in unexpanded **(E)** and expanded **(F)** sections.
747 **H)** Mitochondria area per cell (normalized by soma area). Line reflects median and whiskers are
748 twice the inner quartile range.
749 **I)** The average percent cytoplasm area (soma area - nuclear area) containing mitochondria. Note
750 that ExM better resolves densely packed mitochondria, resulting in greater number, smaller
751 sized, and fewer percent area per cell soma compared with no-ExM.
752 J) Semi quantitative histological scores comparing tested conditions in panels A-D.
753 K-L) Tile scan and high magnification image of mitochondria (cyan) in CA2 neurons and distal
754 dendrites (magenta) with the conditions in F.
755 Scale bars: 50 µm (A,E,F,K), 20 µm (L) and 5 µm (insets).
756
757 **Fig. 5: ProExM pipeline comparison for visualizing Golgi.**
758 **A)** 20X Max-projection image of a section immunostained for GOLGA5 (i) and GFP (iii) pre-
759 ExM with autoclave digestion. (ii) Insets are zoomed images of the dotted box in (i). Images in
760 panels **A-C** were acquired with identical imaging parameters to directly compare conditions.
761 Brightness and contrast were adjusted to the same extent across the entire image.
762 **B)** 20X Max-projection image of a section immunostained for GOLGA5 (i) and GFP (iii) pre-
763 ExM with overnight proteinase K digestion.

764 **C)** 20X Max-projection image of a section immunostained for GOLGA5 (i) and GFP (iii) post-
765 ExM with overnight proteinase K digestion.
766 **D)** 40X Max-projection of a subset of Z sections from an unexpanded section immunostained for
767 GOLGA5 (i) and RFP (iii). Imaging parameters were optimized per condition in **D-E**.
768 **E)** 20X Max-projection of a subset of Z sections from image in (**B**) immunostained pre-ExM
769 with overnight proteinase K digestion. Note the increase in Golgi complexity that is resolved
770 with autoclave or proteinase K digested gels compared with unexpanded sections, although
771 fluorescence intensity was better retained with proteinase K digestion.
772 **F)** Line plot profile showing the fluorescence intensity of unexpanded Golgi (cyan) and Golgi
773 after IHC-pre-ExM with proteinase K digestion (magenta). Measured Golgi are inset in **Diii** and
774 **E.**
775 G-H) Tile scan and high magnification image of GOLGA5 staining in CA2 neurons with the
776 conditions in E. Note the lack of GOLGA5 signal in CA2 dendrites except that from glial cells
777 (asterisk).
778 I) Semi quantitative histological scores comparing tested conditions in panels A-C.
779 Scale bars: 50 µm (Ai, Di, E),10 µm (Aii, Dii), 200 µm (G) and 25 µm (H).
780
781 **Fig. 6: Minimal distortion of tissue or subcellular structures after ProExM**
782 **A-B**) Representative hydrogels from pre-expanded (**A**) and expanded (**B)** horizontal brain
783 sections after 8-hour digestion with proteinase K.
784 **C**) Micro and macro expansion factors from 5 mice. Box plots show the calculated cell body
785 micro expansion factors (see methods) and X denotes the macro expansion factor of the tissue
786 for each hydrogel as measured in B.
787 **D-E**) Representative confocal images of DAPI positive nuclei (grey) and EGFP positive CA2
788 neurons (magenta) in pre-expanded (5X) and expanded (10X) hippocampus after 8-hour
789 digestion with proteinase K.
790 **F**) Root mean square (RMS) error plot calculated from N=3 gels from 3 mice.
791 **G-I**) Representative confocal images of GOLGA5 (grey) immunostaining preExM in 63X
792 unexpanded (**G**) and 20X expanded (**H**) CA2 neurons after 8-hour digestion with proteinase K.
793 The resulting vector plot (**I**) from B-spline image registration. Arrows indicate the direction and
794 magnitude of the transformation required to align the expanded image to the pre-expanded
795 image.
796 Scale bars = 400 µm (**D,E**);10 µm (**G,H**) in pre-expansion dimensions. All images are from the
797 same section from G291.
798
799 **Fig. 7: Resolving dendritic spines with ExM.**
800 **A**) 20X with 3X zoom max-projection image (i) of a section immunostained for RFP pre-ExM
801 with overnight proteinase K digestion. This mouse received 2 tamoxifen injections. (ii) Insets are
802 2X zoomed images of the dotted box in (i). Images were acquired with imaging parameters
803 optimal per condition. Brightness and contrast were adjusted per condition across the entire
804 image.

805 **B**) 40X with 2X zoom max-projection image of an unexpanded tdTomato section. This mouse
806 received 2 tamoxifen injections.
807 **C**) 20X with 2X zoom max-projection image of a section immunostained for GFP pre-ExM with
808 overnight proteinase K digestion.
809 **D**) 40X with 2X zoom max-projection image from an unexpanded section immunostained for
810 GFP. Note the increased background labeling and density of dendritic branches in the
811 unexpanded images, making dendrites more difficult to trace compared with expanded images.
812 Scale bars: 25µm (Ai, Bi, Ci, Di) and 5µm (Aii, Bii, Cii, Dii).
813

REFERENCES

1. Chozinski TJ, Halpern AR, Okawa H, Kim H-J, Tremel GJ, Wong ROL, Vaughan JC. Expansion microscopy with conventional antibodies and fluorescent proteins. Nature Methods. Nature Publishing Group; 2016 Jun;13(6):485–488.

2. Tillberg PW, Chen F, Piatkevich KD, Zhao Y, Yu C-CJ, English BP, Gao L, Martorell A, Suk H-J, Yoshida F, DeGennaro EM, Roossien DH, Gong G, Seneviratne U, Tannenbaum SR, Desimone R, Cai D, Boyden ES. Protein-retention expansion microscopy of cells and tissues labeled using standard fluorescent proteins and antibodies. Nat Biotechnol. 2016;34(9):987–992. PMCID: PMC5068827

3. Asano SM, Gao R, Wassie AT, Tillberg PW, Chen F, Boyden ES. Expansion Microscopy: Protocols for Imaging Proteins and RNA in Cells and Tissues. Curr Protoc Cell Biol. 2018;80(1):e56. PMCID: PMC6158110

4. Ku T, Swaney J, Park J-Y, Albanese A, Murray E, Cho JH, Park Y-G, Mangena V, Chen J, Chung K. Multiplexed and scalable super-resolution imaging of three-dimensional protein localization in size-adjustable tissues. Nat Biotechnol. 2016;34(9):973–981. PMCID: PMC5070610

5. Park H-E, Choi D, Park JS, Sim C, Park S, Kang S, Yim H, Lee M, Kim J, Pac J, Rhee K, Lee J, Lee Y, Lee Y, Kim S-Y. Scalable and Isotropic Expansion of Tissues with Simply Tunable Expansion Ratio. Adv Sci (Weinh). 2019 Nov;6(22):1901673. PMCID: PMC6864509

6. Gambarotto D, Zwettler FU, Le Guennec M, Schmidt-Cernohorska M, Fortun D, Borgers S, Heine J, Schloetel J-G, Reuss M, Unser M, Boyden ES, Sauer M, Hamel V, Guichard P. Imaging cellular ultrastructures using expansion microscopy (U-ExM). Nat Methods. 2019;16(1):71–74. PMCID: PMC6314451

7. Katoh Y, Chiba S, Nakayama K. Practical method for superresolution imaging of primary cilia and centrioles by expansion microscopy using an amplibody for fluorescence signal amplification. Mol Biol Cell. 2020 15;31(20):2195–2206. PMCID: PMC7550703

8. Shi X, Li Q, Dai Z, Tran AA, Feng S, Ramirez AD, Lin Z, Wang X, Chow TT, Seiple IB, Huang B. Label-retention expansion microscopy. bioRxiv. Cold Spring Harbor Laboratory; 2019 Jul 2;687954.

9. Truckenbrodt S, Sommer C, Rizzoli SO, Danzl JG. A practical guide to optimization in X10 expansion microscopy. Nature Protocols. Nature Publishing Group; 2019 Mar;14(3):832–863.

10. Chen F, Tillberg PW, Boyden ES. Expansion microscopy. Science. 2015 Jan 30;347(6221):543–548. PMID: 25592419

11. Richardson DS, Lichtman JW. Clarifying Tissue Clearing. Cell. 2015 Jul 16;162(2):246–257. PMCID: PMC4537058

851 12. Wassie AT, Zhao Y, Boyden ES. Expansion microscopy: principles and uses in biological
852 research. Nat Methods. 2019;16(1):33–41. PMCID: PMC6373868

853 13. Kunz TC, Götz R, Gao S, Sauer M, Kozjak-Pavlovic V. Using Expansion Microscopy to
854 Visualize and Characterize the Morphology of Mitochondrial Cristae. Front Cell Dev Biol.
855 2020;8:617. PMCID: PMC7373753

856 14. Büttner M, Lagerholm CB, Waithe D, Galiani S, Schliebs W, Erdmann R, Eggeling C,
857 Reglinski K. Challenges of Using Expansion Microscopy for Super-resolved Imaging of
858 Cellular Organelles. Chembiochem. 2020 Oct 13; PMID: 33049107

859 15. Pesce L, Cozzolino M, Lanzanò L, Diaspro A, Bianchini P. Measuring expansion from
860 macro- to nanoscale using NPC as intrinsic reporter. J Biophotonics. 2019 Aug;12(8).
861 PMCID: PMC7065622

862 16. Sun D, Fan X, Zhang H, Huang Z, Tang Q, Li W, Bai J, Lei X, Chen X. Click-ExM enables
863 expansion microscopy for all biomolecules. bioRxiv. Cold Spring Harbor Laboratory; 2020
864 Mar 20;2020.03.19.998039.

865 17. Pernal SP, Liyanaarachchi A, Gatti DL, Formosa B, Pulvender R, Kuhn ER, Ramos R, Naik
866 AR, George K, Arslanturk S, Taatjes DJ, Jena BP. Nanoscale imaging using differential
867 expansion microscopy. Histochem Cell Biol. 2020 Jun;153(6):469–480. PMID: 32193594

868 18. Zhao Y, Bucur O, Irshad H, Chen F, Weins A, Stancu AL, Oh E-Y, DiStasio M, Torous V,
869 Glass B, Stillman IE, Schnitt SJ, Beck AH, Boyden ES. Nanoscale imaging of clinical
870 specimens using pathology-optimized expansion microscopy. Nat Biotechnol. 2017
871 Aug;35(8):757–764. PMCID: PMC5548617

872 19. Götz R, Panzer S, Trinks N, Eilts J, Wagener J, Turrà D, Di Pietro A, Sauer M, Terpitz U.
873 Expansion Microscopy for Cell Biology Analysis in Fungi. Front Microbiol. 2020;11:574.
874 PMCID: PMC7147297

875 20. Düring DN, Rocha MD, Dittrich F, Gahr M, Hahnloser RHR. Expansion Light Sheet
876 Microscopy Resolves Subcellular Structures in Large Portions of the Songbird Brain. Front
877 Neuroanat. 2019;13:2. PMCID: PMC6365838

878 21. Jiang N, Kim H-J, Chozinski TJ, Azpurua JE, Eaton BA, Vaughan JC, Parrish JZ.
879 Superresolution imaging of Drosophila tissues using expansion microscopy. Mol Biol Cell.
880 2018 15;29(12):1413–1421. PMCID: PMC6014096

881 22. Cahoon CK, Yu Z, Wang Y, Guo F, Unruh JR, Slaughter BD, Hawley RS. Superresolution
882 expansion microscopy reveals the three-dimensional organization of the Drosophila
883 synaptonemal complex. Proc Natl Acad Sci U S A. 2017 Aug 15;114(33):E6857–E6866.
884 PMCID: PMC5565445

885 23. Gao R, Asano SM, Upadhyayula S, Pisarev I, Milkie DE, Liu T-L, Singh V, Graves A,
886 Huynh GH, Zhao Y, Bogovic J, Colonell J, Ott CM, Zugates C, Tappan S, Rodriguez A,
887 Mosaliganti KR, Sheu S-H, Pasolli HA, Pang S, Xu CS, Megason SG, Hess H, Lippincott-

888 Schwartz J, Hantman A, Rubin GM, Kirchhausen T, Saalfeld S, Aso Y, Boyden ES, Betzig
889 E. Cortical column and whole-brain imaging with molecular contrast and nanoscale
890 resolution. Science. 2019 Jan 18;363(6424).

891 24. Fecher C, Trovò L, Müller SA, Snaidero N, Wettmarshausen J, Heink S, Ortiz O, Wagner I,
892 Kühn R, Hartmann J, Karl RM, Konnerth A, Korn T, Wurst W, Merkler D, Lichtenthaler SF,
893 Perocchi F, Misgeld T. Cell-type-specific profiling of brain mitochondria reveals functional
894 and molecular diversity. Nature Neuroscience. 2019 Oct;22(10):1731–1742.

895 25. Karagiannis ED, Kang JS, Shin TW, Emenari A, Asano S, Lin L, Costa EK, Consortium
896 IGC, Marblestone AH, Kasthuri N, Boyden ES. Expansion Microscopy of Lipid Membranes.
897 bioRxiv. Cold Spring Harbor Laboratory; 2019 Nov 4;829903.

898 26. Martínez GF, Gazal NG, Quassollo G, Szalai AM, Cid-Pellitero ED, Durcan TM, Fon EA,
899 Bisbal M, Stefani FD, Unsain N. Quantitative expansion microscopy for the characterization
900 of the spectrin periodic skeleton of axons using fluorescence microscopy. Sci Rep. 2020
901 19;10(1):2917. PMCID: PMC7031372

902 27. Scheible MB, Tinnefeld P. Quantifying Expansion Microscopy with DNA Origami
903 Expansion Nanorulers. bioRxiv. Cold Spring Harbor Laboratory; 2018 Feb 14;265405.

904 28. Vanheusden M, Vitale R, Camacho R, Janssen KPF, Acke A, Rocha S, Hofkens J.
905 Fluorescence Photobleaching as an Intrinsic Tool to Quantify the 3D Expansion Factor of
906 Biological Samples in Expansion Microscopy. ACS Omega. 2020 Mar 17;5(12):6792–6799.
907 PMCID: PMC7114699

908 29. Min K, Cho I, Choi M, Chang J-B. Multiplexed expansion microscopy of the brain through
909 fluorophore screening. Methods. 2020 01;174:3–10. PMID: 31326595

910 30. Chang J-B, Chen F, Yoon Y-G, Jung EE, Babcock H, Kang JS, Asano S, Suk H-J, Pak N,
911 Tillberg PW, Wassie AT, Cai D, Boyden ES. Iterative expansion microscopy. Nat Methods.
912 2017 Jun;14(6):593–599. PMCID: PMC5560071

913 31. Zwettler FU, Reinhard S, Gambarotto D, Bell TDM, Hamel V, Guichard P, Sauer M.
914 Molecular resolution imaging by post-labeling expansion single-molecule localization
915 microscopy (Ex-SMLM). Nat Commun. 2020 Jul 7;11(1):3388. PMCID: PMC7340794

916 32. Steward O, Schuman EM. Protein synthesis at synaptic sites on dendrites. Annu Rev
917 Neurosci. 2001;24:299–325. PMID: 11283313

918 33. Pierce JP, Mayer T, McCarthy JB. Evidence for a satellite secretory pathway in neuronal
919 dendritic spines. Curr Biol. 2001 Mar 6;11(5):351–355. PMID: 11267872

920 34. Bowen AB, Bourke AM, Hiester BG, Hanus C, Kennedy MJ. Golgi-independent secretory
921 trafficking through recycling endosomes in neuronal dendrites and spines. Elife. 2017 06;6.
922 PMCID: PMC5624785

923 35. Kennedy MJ, Ehlers MD. ORGANELLES AND TRAFFICKING MACHINERY FOR
924 POSTSYNAPTIC PLASTICITY. Annual Review of Neuroscience. 2006 Jul 21;29(1):325–
925 362.

926 36. Alexander GM, Brown LY, Farris S, Lustberg D, Pantazis C, Gloss B, Plummer NW, Jensen
927 P, Dudek SM. CA2 neuronal activity controls hippocampal low gamma and ripple
928 oscillations. Elife. 2018 02;7. PMCID: PMC6251629

929 37. Schindelin J, Arganda-Carreras I, Frise E, Kaynig V, Longair M, Pietzsch T, Preibisch S,
930 Rueden C, Saalfeld S, Schmid B, Tinevez J-Y, White DJ, Hartenstein V, Eliceiri K,
931 Tomancak P, Cardona A. Fiji: an open-source platform for biological-image analysis. Nat
932 Methods. 2012 Jun 28;9(7):676–682. PMCID: PMC3855844

933 38. Shamonin DP, Bron EE, Lelieveldt BPF, Smits M, Klein S, Staring M, Alzheimer's Disease
934 Neuroimaging Initiative. Fast parallel image registration on CPU and GPU for diagnostic
935 classification of Alzheimer's disease. Front Neuroinform. 2013;7:50. PMCID: PMC3893567

936 39. Klein S, Staring M, Murphy K, Viergever MA, Pluim JPW. elastix: A Toolbox for Intensity-
937 Based Medical Image Registration. IEEE Transactions on Medical Imaging. 2010
938 Jan;29(1):196–205.

939